The City College

City University of New York

New York, N.Y. 10031.

Technical Report

(NASA-CR-153077) THE DETERMINATION OF SURFACE ALBEDO FROM METEOROLOGICAL SATELLITES (City Coll. of the City Univ. of New York.) 41 p HC A03/MF A01 CSCL 03B

N77-24566

Unclas G3/43 29172

The Determination of Surface Albedo from Meteorological Satellites

Winthrop T. Johnson

June 1, 1977.

Grant NGR 33-013-086

NASA, Goddard Space Flight Center

Abstract

Surface albedo measurements have, in the past, been taken mainly near the earth's surface and from aircraft. In this study a surface albedo was determined from visible data collected by the NOAA-4 polar orbiting meteorological satellite. In order to filter out the major cause of atmospheric reflectivity, namely clouds, techniques were developed and applied to the data resulting in a map of global surface albedo. Neglecting spurious surface albedos for regions with persistent cloud cover, sun glint effects, insufficient reflected light and, at this time, some unresolved influences, the surface albedos retrieved from satellite data closely matched those of a global surface albedo map produced from surface and aircraft measurements and from characteristic albedos for land type and land use.

Table of Contents

List of Figures

Introduction

The albedo of an object is a measure of its light-reflecting property. Usually expressed in percent, the surface albedo is the ratio of the amount of reflected radiation per unit area to the total amount of incoming incident radiation per unit area.

Reflectivity is a function of the nature of the surface, the angle of incidence, and the angle from which the measurement is taken. For liquids such as the oceans, reflectivity varies with depth, turbidity, surface roughness and current velocity. Albedos for solids such as snow, vegetation, and soil, vary with color, texture, wetness, grain size, and, in the case of snow, age. Therefore, due to the inhomogeneity of the surface, the earth's albedos range from small values, e.g., 6 to 9% for oceanic regions near the Equator, to large percentages, e.g., 70 to 95% for fresh fallen snow. Both changes in the solar zenith angle and (because of non-diffuse reflective surface properties) changes in the angle from which the reflective measurement is made also affect the measured albedo.

Prior to the advent of meteorological satellites, albedo measurements were taken exclusively near the surface and from aircraft. These produced both regional and global maps of surface albedo (Kung, Bryson and Lenschow, 1964; Posey and Clapp, 1964).

With the introduction of satellites as meteorological observatories, global maps were first produced from vidicon (television) camera measurements (Winston and Taylor, 1967; Taylor and Winston, 1968; Winston, 1971) and then from radiometric measurements (Raschke and Bandeen, 1970; Vonder Haar and Suomi, 1971; Gruber, 1973; Flanders and Smith, 1975). However, these maps are of planetary rather than surface albedo, the difference being that planetary albedo is a measure of the earth-atmospheric reflectivity which includes effects of reflectance, scattering and absorption by air molecules, aerosols and clouds.

The major atmospheric influence on satellite measurements in the visible spectrum is the highly reflective nature of clouds. It is the aim of this study to develop techniques for filtering out cloud reflectance from satellite measurements in order to retrieve surface albedo quantities. Moreover, a global surface albedo array derived by these techniques has been constructed from five days of satellite data and evaluated in comparison to other such arrays and characteristic surface albedo values. These techniques have been computerized by the author so that weekly, monthly, seasonally, or yearly climatologies of global surface albedo can be generated.

Development of surface albedo arrays would contribute to many areas in meteorological research. For instance, the surface albedo is one of the essential components in radiation and heat budget investigations. Since differential heating of the earth's surface provides the energy to drive the circulation of the atmosphere, the global surface albedo distribution is directly related to atmospheric circulation energetics. In atmospheric simulation models, such as the Goddard Institute for Space Studies (GISS) global atmospheric circulation model (Sommerville et al., 1974), a global surface albedo is one of the input arrays necessary to run the model. Better surface albedo specification would presumably lead to better results in these areas.

On the question of whether or not global atmospheric models are sensitive to changes in surface albedo, tests have been conducted at GISS with the GISS global atmospheric model by Drs. W. Quirk and Y. Sud (1976) and analyzed by the author. Two five day forecasts were produced using the same initial conditions, but different global surface albedo arrays. A climatological January global surface albedo array from Schutz and Gates (1972) was used in one forecast and a daily updated array in the other. This latter array was also initialized from the Schutz and Gates array but changed to correspond to the weekly average snow and ice boundary map produced by the Satellite Applications Group of NESS (NOAA)[1]. It was

1. The National Environmental Satellite Service (NESS) of the National Oceanic and Atmospheric Administration. (NOAA).

updated daily using a functional relationship between the model's forecast snow depth and surface albedo. After five days, surface temperature differences of 5° to 15°F and sea level pressure differences of 4 mb. occurred in both the U.S. and Canada in regions of systematic, non-random differences in albedo. These results indicate not only model sensitivity to albedo variations, but also a possible impact on forecast performance.

Data Source

The data for this study are derived from measurements taken by the scanning radiometer aboard the NOAA 4 meteorological satellite (Environmental Satellite Imagery, Feb. 1976; Fortuna and Hambrick, 1974; Conlan, 1973; Schwalb, 1972). The NOAA 4 is a sun-synchronous, near circular, polar-orbiting satellite completing one orbit every 115 minutes. It transits the Equator on the descending node (southbound) at approximately 0900 hours local time and at approximately 2100 hours local time on the ascending node (northbound).

The two-channel scanning radiometer measures energy in both the visible (0.5 to 0.7 μm.) and the infrared (10.5 to 12.5 μm.) spectral ranges, scanning from horizon to horizon across the orbital path or track. Preflight calibration consisted of correlating the response of the radiometer to a brightness source of known spectral energy output. The only onboard calibration is a baseline determination when the radiometer scans empty space.

For the visible channel the instantaneous field of view is a 4 km. square at the nadir (subsatellite point), increasing to a rectangle 7.5 km. by 15 km. at a horizontal distance 1668 km. from the nadir. At the subsatellite point there is a 4 km. gap between successive crosstrack swaths of data which disappears more than 1385 km. from the subpoint. Swaths of data from successive orbits overlap 1668 km. from nadir (satellite observation angle of approximately 60°) at the Equator. This distance from the subpoint decreases with increasing latitude. Forward movement of the spacecraft combined with crosstrack scanning provides global visible measurements every 12 or 13 orbits.

The brightness measurements taken by the visible channel of the scanning radiometer are recorded by an onboard magnetic tape recorder. This analog signal is later transmitted to one of two ground receiving stations and retransmitted to NESS in Suitland, Maryland for processing.

Processing includes earth location, normalization, digitation, cropping and mapping. Each data spot must be earth located in order to determine the solar zenith angle at the time of observation for that spot. The data are then normalized to an overhead sun using a cosine function factor of the solar zenith angle. The analog signal is converted into digital brightness counts from zero to 254. This is a linear conversion whereby each digital count represents a range of 40 foot lamberts (i.e., digital brightness count 0 represents 0 to 39 foot lamberts, etc.). Digital brightness count 255 is used for missing data.

Gaps in the data stream occur periodically off the Eastern U.S. coast near Bermuda due to insufficient data recording capabilities of the onboard recorder, the location of the two ground receiving stations, and shifting orbital tracks.

For mapping purposes, one day of data, beginning with the orbital pass where the satellite transits the Equator at approximately 0700Z, is grouped together. In regions where data are collected from more than one pass, the latest data are retained. This results in lines of discontinuty on visual displays between data retained from successive passes, and especially between data retained from the first and last pass of the day. The digitized data are then placed into two 2048 X 2048 square grids, each overlaying a hemispheric polar stereographic map. These are made available on magnetic tape through the Satellite Data Services Branch of the National Climatic Center. Data for five days, January 31 through February 4, 1976, have been used in this study.

At the time this data set was being processed, the digital code for missing data, 255, was not being inserted into polar grid points which had a solar zenith angle equal to or greater than 90°. Any brightness recorded by the radiometer, whether real or spurious was left intact in the data stream. This resulted in non zero digital counts, usually multiples of 10, for grid points in the polar night region. Photographic and facsimile maps exhibit a spotty appearance in these regions due to this non zero field.

This same spotty appearance occurs on maps over portions of Antarctica and the Weddell Sea, northern Russia and Scandinavia for the days studied. Again the reason for this is an insufficient amount of reflected light. These areas are scanned on the last orbital pass for that day, thus all the data collected, no matter how far away from the satellite (i.e., large satellite observation angles) are mapped. Any previous measurements for this region from earlier passes are simply deleted. Since the satellite overflies a region in the morning its crosstrack scanner measures regions "toward" the sun and "away" from the sun. Regions viewed "away" from the sun would have a greater solar zenith angle. This larger solar zenith angle coupled with the retention of all data on the last pass leads to saving data collected in the polar regions with insufficient illumination.

Method of Analysis

The data on tape are in digitized counts of reflected brightness from both the surface and the atmosphere. To retrieve a surface reflected brightness the atmospheric reflected brightness must be filtered out. Since clouds are the major contributors to atmospheric reflection of visible light, techniques were developed and applied to the data to filter out this cloud effect. No attempt was made at this time to filter out the less influential atmospheric effects such as reflectivity due to atmospheric aerosols or Rayleigh scattering.

The earth's surface was assumed to be an isotropic surface (i.e., with no preferential direction of reflected energy) thereby eliminating the effect of measurements taken at different satellite observation angles and solar zenith angles. This assumption was also used by Winston and Taylor (1967), Taylor and Winston (1968), and Flanders and Smith (1975), for studies of brightness, long wave radiation and albedo.

The cloud filtering technique was based on the premise that clouds increase the amount of light reflected back to space. For example, over a dark surface the brightness count for a particular grid point is higher on a cloudy day than on a cloudless day. In this study, groups of grid point brightness counts were analyzed in the form of histograms. An increase in the modal brightness value is generally observed on cloudy versus cloudless days. As sky conditions change from clear to thin cirrostratus to lower, thicker stratus, the modal brightness also shifts to higher brightness values. Overcast stratiform cloud conditions over the analyzed region gave only one brightness peak. Open and closed cellular cumulus, cumulonimbus and regions only partially overlain by clouds resulted in bimodal histograms. In this later case, the lower end peak, (i.e., the peak with the lower brightness count) and adjacent brightness counts were taken to represent the surface reflectivity. The higher end peak presumably represented cloud reflection.

The first cloud filtering technique employed was developed to eliminate any higher brightness peaks and save only the lower surface representative peak. In order to carry out a low end modal searching process the hemispheric data (2048 X 2048 grid points) were regrouped into square grid boxes consisting of 80 grid points on a side (approximately 800 km.). This formed a 25 X 25 grid box array for each hemisphere. A histogram of brightness counts versus frequency was then constructed[2] from the 6400 grid point values for each grid box. As an example, figure 1 is a histogram constructed from one grid box over the

2. A special computer program was designed to automate construction of the histogram, as well as the search for modal brightness, and determination of characteristic surface albedos. The Fortran code for the program is given in the Appendix.

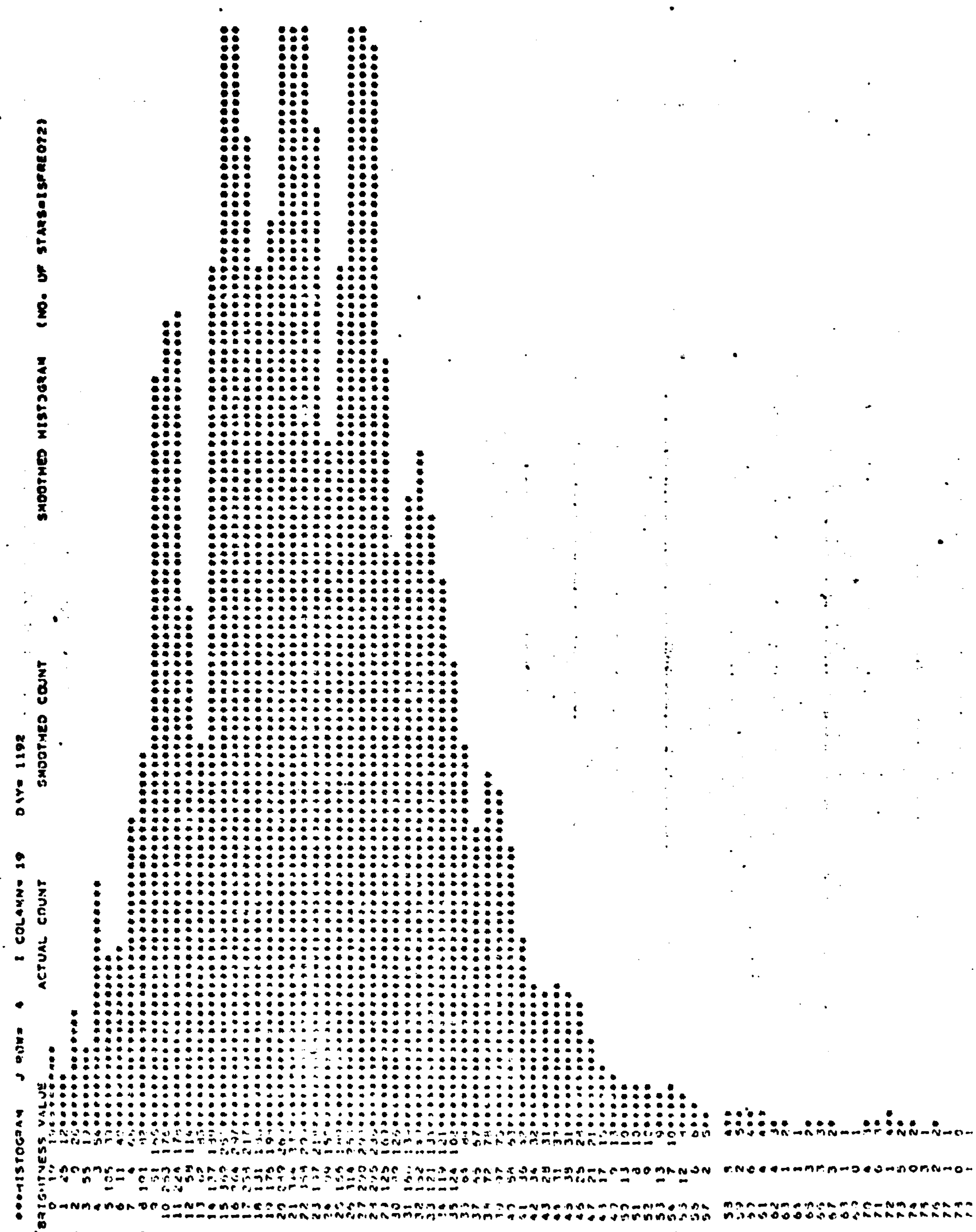

Fig.1. Histogram of brightness counts versus smoothed frequencies for one grid box over the Indian Ocean. The lowest, middle and highest row of numbers are the brightness counts, actual frequencies and smoothed frequencies respectively. Each star represents two smoothed frequencies.

Indian Ocean. The bottom row of numbers are the brightness counts from zero to 255. Above these are the corresponding frequencies or number of values of that brightness measured within the grid box. For instance, for brightness value 16 there are 264 measurements of a 16 brightness count out of 6400 total measurements. A three point smoothing operator of the following form was used on brightness values 2 through 253 to reduce the "noise" in the histogram:

$$SF_n = 1/3(F_{n-1} + F_n + F_{n+1})$$

where

SF_n = smoothed frequency for brightness count n.

F_n = frequency of brightness count n.

$F_{n \pm 1}$ = frequency of brightness count n $\pm$ 1.

Again using brightness count 16 as an example, the frequencies of brightness count 15, 16 and 17 (369, 264 and 258 respectively) are added together and then divided by 3 to give the smoothed frequency for brightness count 16 (i.e., 297). A two point smoother was applied to brightness values 1 and 254 with the next higher and lower brightness counts respectively.

In other words the actual frequencies of brightness counts 1 and 254 were added to brightness counts 2 and 253 and then divided to 2 to give smoothed frequencies for brightness counts 1 and 254.

The smoothed frequencies in figure 1 appear in a row just above the actual frequencies. The stars are used to give a more graphic representation of the smoothed frequencies for each brightness count. Each star represents 2 frequencies up to a possible 240 frequencies (i.e., 120 stars).

Initially a mode was determined from the lowest 35% of the data (i.e., frequencies being added together starting with brightness count 1 and reaching 35% of the data). However, for regions of clear skies the low end mode did not correspond to the mode for the entire histogram. It did correspond to the lower end mode in the bimodal case. Modes from clear sky regions were studied and an empirical relationship was derived between the mode and the beginning of the peak (basically, the first brightness count with a frequency of 4 or more). This range was then used as a criterion to distinguish modes of clear skies from modes of partly cloudy skies for modal values from more than 35% of the data. Modes from the first 80% of the data and then from 10% less data down to 50% and then 5% less data to 40% were checked against the range criterion for clear skies. The first mode which had a range within the limiting criterion or the mode for the lowest 35% of the data was saved. This mode was then used in calculating a mean brightness.

In figure 1 a low end modal search process was carried out for the first 80% of the smoothed frequencies. The modal brightness value was 21 with a mode of 330 smoothed frequencies. The range between the modal brightness value and the first brightness value of four or more (i.e., brightness count 1 in this case) is 21 which is less than the clear skies criterion and so no further low end modal searching with successively smaller percentages of data was conducted. Next the number of brightness counts between the mode and the beginning of the brightness peak was added to the modal brightness count and used to define the end of the brightness peak. In figure 1 the number of brightness counts between the modal brightness count of 21 and the beginning of the brightness peak, namely brightness count 1, were computed. This range of 20 was then added onto the modal brightness count in order to designate the end of the brightness peak. Brightness count 41 was thus defined as the end of the brightness peak in this case. A mean brightness count was calculated from smoothed frequencies of brightness count 1 to the brightness count marking the end of the brightness peak. The mean brightness count was 21.8 for figure 1. These mean brightness counts represent the mean surface brightness for that grid box. Surface representative means were calculated for each grid box for each of the five days.

These means, however, are in terms of brightness counts representing specified internals of energy expressed in foot lamberts. To convert these means into albedo measurements, each value must be multiplied by a constant conversion factor derived by Gruber (1974). It takes into account a solar constant of 1.94 $ly.min.^{-1}$ and the percentage of total incoming solar radiation effectively sensed in the visible spectral range of the radiometer.

The first cloud filtering technique was used to capture a surface representative mode for clear or partly cloudy sky conditions. A second filtering technique had to be applied to the data to eliminate means from regions with overcast conditions where the satellite could not effectively "see" the earth's surface. A five day minimum scanning procedure based on the work of McClain and Baker (1969) in the reduction of cloud contamination in snow brightness measurements and snow boundary delineation for satellite data was used. A similar multiday minimum scanning procedure was used by Chen (1975) for monthly minimum planetary albedo mapping from satellite data.

From five days of calculated mean albedos for each grid box only the lowest mean albedo was retained as the surface representative albedo. In this final scanning procedure the means had to have been calculated from a sample of at least 2000 frequencies, that is, the number of smoothed frequencies from brightness count 1 to the brightness count marking the end of the modal peak had to exceed 1999. This eliminated the cases where the low end mode occurred very close to the beginning of the peak thus giving a lower than representative mean.

Results

Hemispheric surface albedo maps generated from the application of two cloud filtering techniques on five consecutive days, January 31 to February 4, 1967, are given in figures 2 and 4. The 25 X 25 grid overlaying the geographical hemispheric map shows the boundaries of each grid box. The lowest surface representative mean albedo (which passes the limiting criteria) for the five days is written in each box. An I for any box denotes insufficient light occurred in the northern hemisphere in the polar night region and in both hemispheres due to the retention of all data from the last pass. A 99 found in four of the grid boxes in the northern hemisphere means that no surface representative albedo was determined from the data. The reasons for this will be discussed later.

For most grid boxes the albedos are close to characteristic surface albedos for specific types of surfaces. Albedos for water surfaces generally fell in the 5 to 12% range with higher albedos in the higher northern latitudes. Non snow and ice covered land regions had albedos of from 7 up to 35% in desert regions. Snow and ice covered areas exhibited higher albedos than its characteristic non covered form. Albedos for Antarctica were from 80 to 91%. It must be noted that the scanning radiometer was only able to distinguish a reflective brightness up to a corresponding 91% albedo. At this point the instrument was "saturated".

Besides a relative closeness of most computed albedos to the characteristic surface albedos, some computed values showed discrepancies. For these grid boxes daily hemispheric photographs produced from the same scanning radiometer data were studied. The first problem was one of persistant cloud cover over the grid box for the five days. This did not necessarily mean an overcast condition over the entire grid box. Boxes with as low as 7 tenths sky cover produced unusually high albedos. These albedos have been labeled on the maps with a bar to denote persistant cloud cover and do not represent a surface albedo.

Other grid boxes with unusually high albedos were a result of clouds and sun glint. Sun glint occurs only over the water and appears as a bright area. This mirror effect happens when the viewing angle is equal to the angle of incidence of the sunlight. In the photographs this takes the form of bright swaths along the satellite track or bright spots. Albedos recorded for these regions are generally around 35%. A combination of cloudy days, missing data for one or more days, and the occurrence of sun glint on the day with the lowest mean albedo for that region, produced higher than expected albedos.

The reason for unusually higher albedos from some grid boxes is not as clear. In these cases clouds were present covering less than 7 tenths of the grid box area on the day of lowest mean albedo. These are denoted by a filled in triangle in the lower right corner of the grid square. Further study needs to be conducted to determine why the high albedos are present and how to correct this situation in the computer program.

One further point should be kept in mind when viewing the surface representative albedo maps. When a grid box covers two or more types of surfaces the lower albedo (provided enough cases for that surface are present) will represent the entire grid box. The most numerous example of this is for grid boxes covering both land and water. If the water has a lower albedo as is usually the case then the albedo for the water would represent the entire grid box. However, if clouds covered the water for the five days then the land albedo would be retained.

A comparison between global surface albedo arrays derived from characteristic albedos for surface types, from readings taken near the ground and from aircraft, and the global surface albedo array derived from satellite data follows.

Posey and Clapp (1964) compiled four monthly average global surface albedo maps drawing exclusively upon the work of Budyko (1958) for open ocean values and defining characteristic albedos for different land use types and surface conditions for non open ocean areas. The average January surface albedo map, figures 3 and 5 will be used for comparison.

Southern Hemisphere

Discounting grid boxes with persistent cloudiness, sun glint and unresolved errors, the satellite albedos derived for the open oceans exhibit a fairly good agreement with Posey and Clapp. The range is from 5 to 12% as opposed to 6 to 9% for Posey and Clapp. The satellite derived maps show more geographical fluctuation owing to the fact that these are five day minimums rather than monthly means. The systematic stepwise increase in albedo found in Posey and Clapp is not present in the satellite derived maps.

Antarctic albedos are generally higher, 80 to 91% than the near uniform 80% albedos of Posey and Clapp. Four grid boxes in the eastern section of the continent which cover both land and water depict the case where the land albedo is higher than the water since the water is covered by persistent clouds. The retrieved albedo would then be the lower, cloud albedo for these cases. Thus these boxes are marked for further study.

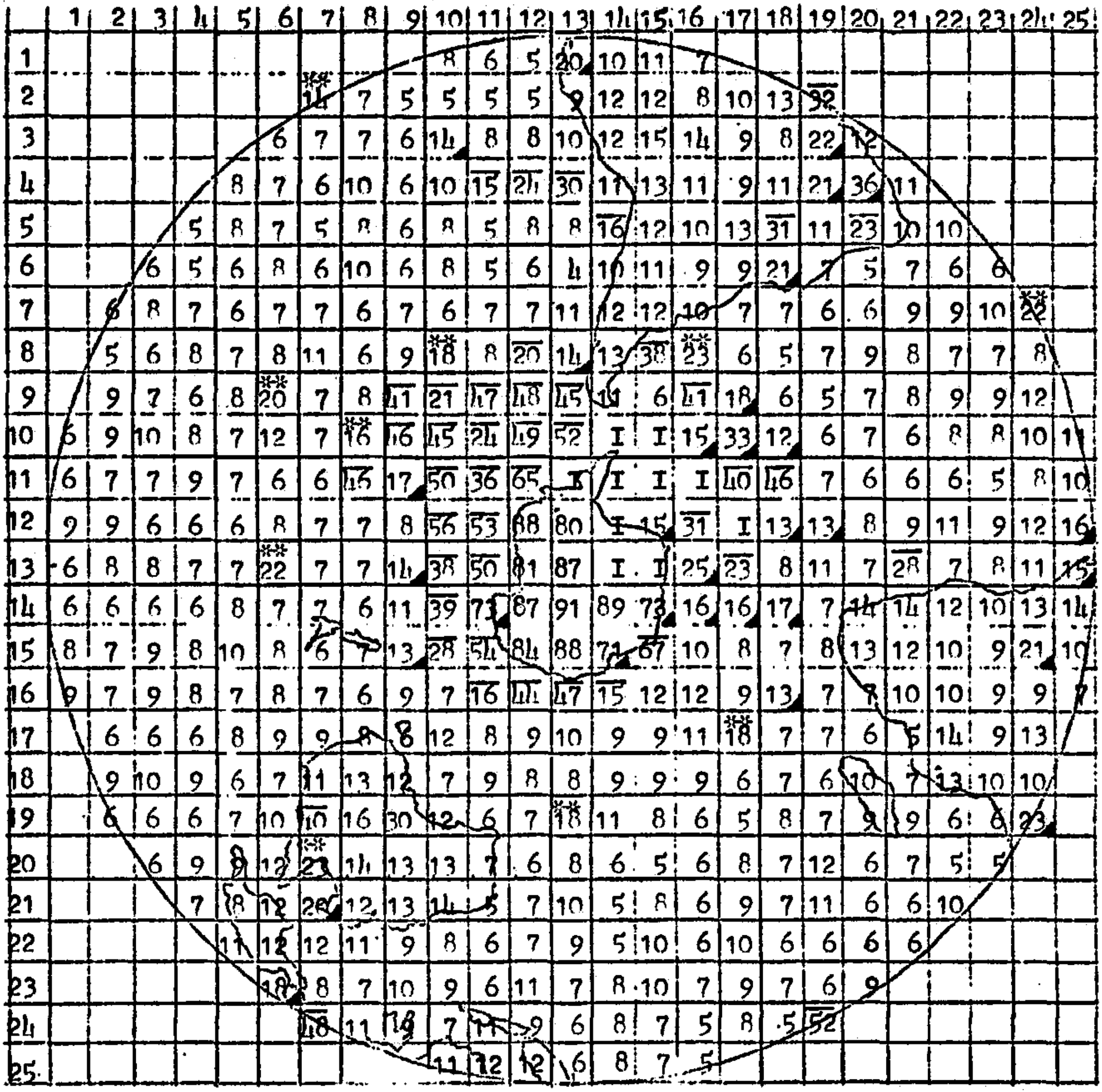

Fig.2. Surface albedos derived from satellite data, January 31 - February 4, 1976, Southern Hemisphere. Albedos are given in percent. A bar over an albedo indicates persistent cloud cover over five days. A double asterisk above an albedo indicates sun glint contamination. A ◢ in the lower right corner of the grid box means that the albedo was unrepresentative for reasons as yet unclear.

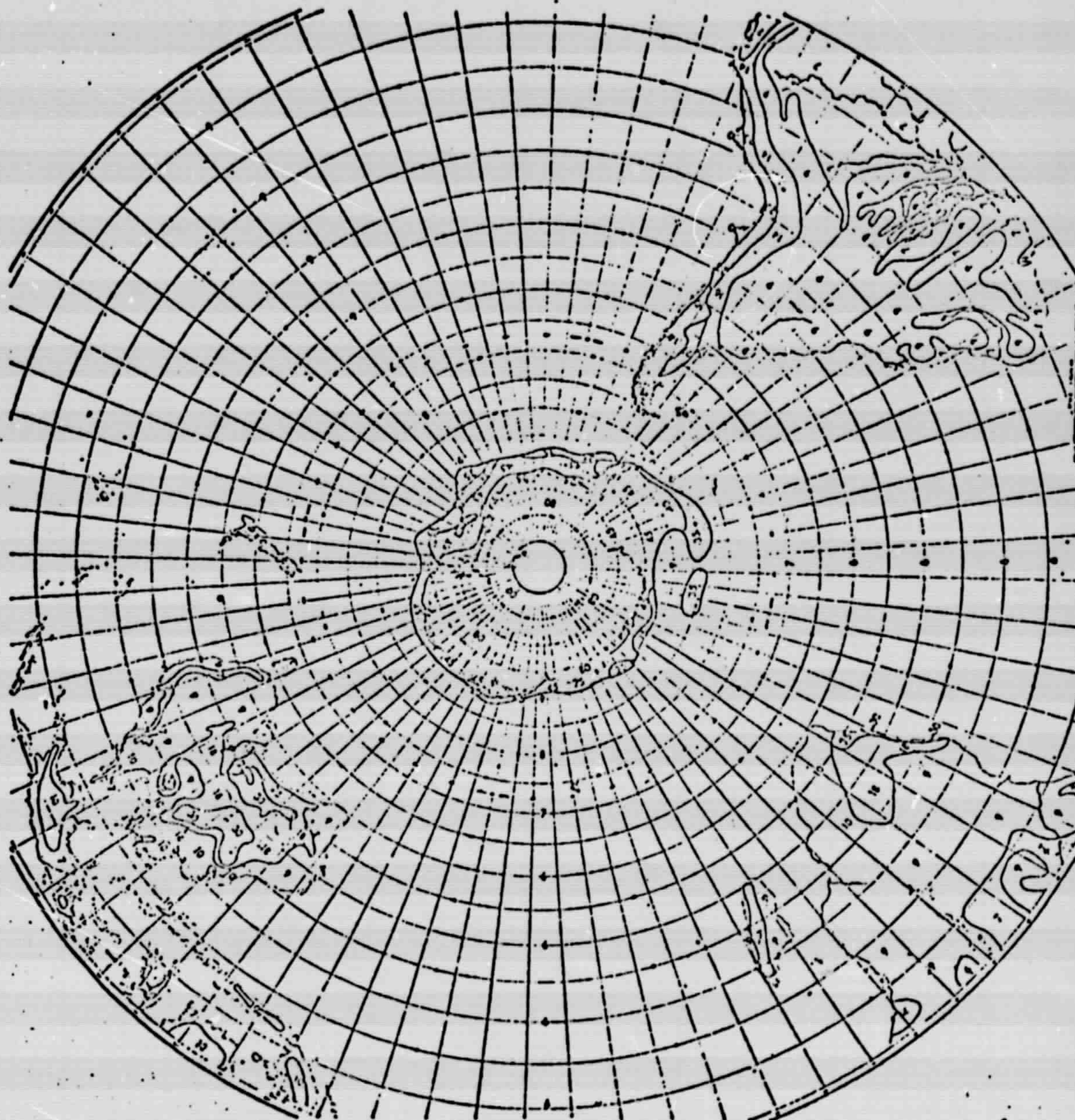

Fig.3. Normal surface albedo, January, Southern Hemisphere. Solid lines in Antarctic waters are northern boundary of pack ice (heavy) or boundary of ice regions (light). No snow boundary indicated. Numbers are albedo in percent. (Taken from Posey and Clapp).

Australian albedos do not show the large range of albedos found in Posey and Clapp. Numerous reasons for these differences such as grid size, solar zenith angle at time of observation, uncharacteristic soil wetness, changes in land use since 1964, etc., could be ascribed for these differences but the cause(s) is unclear at this time.

Agreement is very close, 7 to 13% compared to 7 to 10%, for most albedos in Southern Africa. The portion of Southwestern Africa with albedos from 18 to 30% is not appearant on the satellite derived map.

Slightly higher albedos, up to 5% occur over most of South America except along the western coast.

Northern Hemisphere

Most open water albedos are again close to those given by Posey and Clapp. Fluctuations of albedos for the same latitude still exist, however, at high latitudes the increase of albedo with increasing latitude is found in both maps in the North Atlantic and North Pacific oceans.

High albedos from 49 to 59% due to sea ice are found in three grid boxes: one covering the Bering Straits, another extending from the southwestern edge of Greenland across to Labrador and a third in the Shelikhov Gulf, north of the Sea of Okhotsk between Siberia and the Kamchatka Penninsula. In order to verify the existence of sea ice in these areas at the time the observations were made,

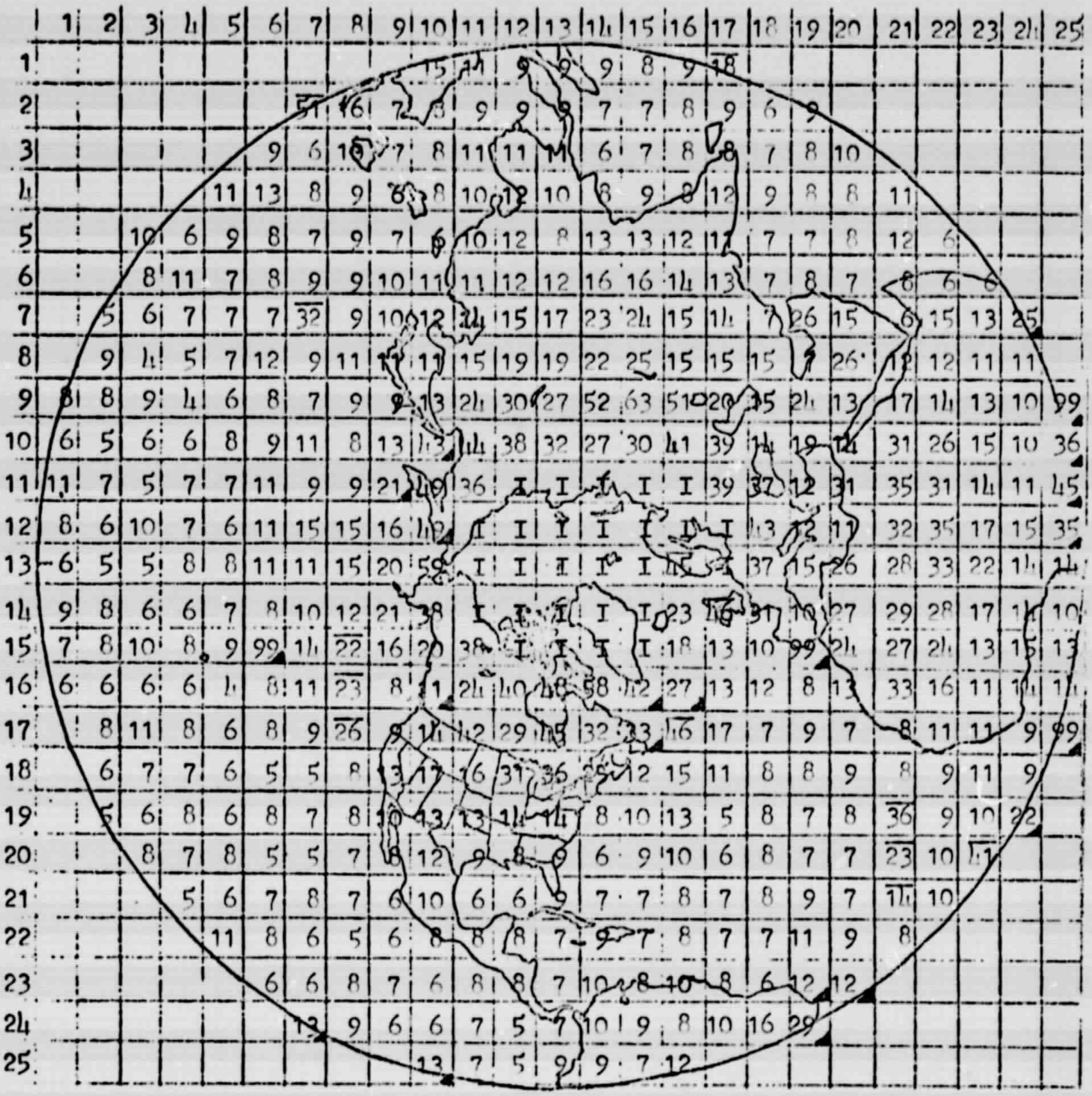

Fig.4. Surface albedos derived from satellite data, January 31 - February 4, 1976, Northern Hemisphere. Albedos are given in percent. A bar over an albedo indicates persistent cloud cover over five days. A double asterisk above an albedo indicates sun glint contamination. A ◢ in the lower right corner of the grid box means that the albedo was unrepresentative for reasons as yet unclear. An albedo of 99 represents missing data.

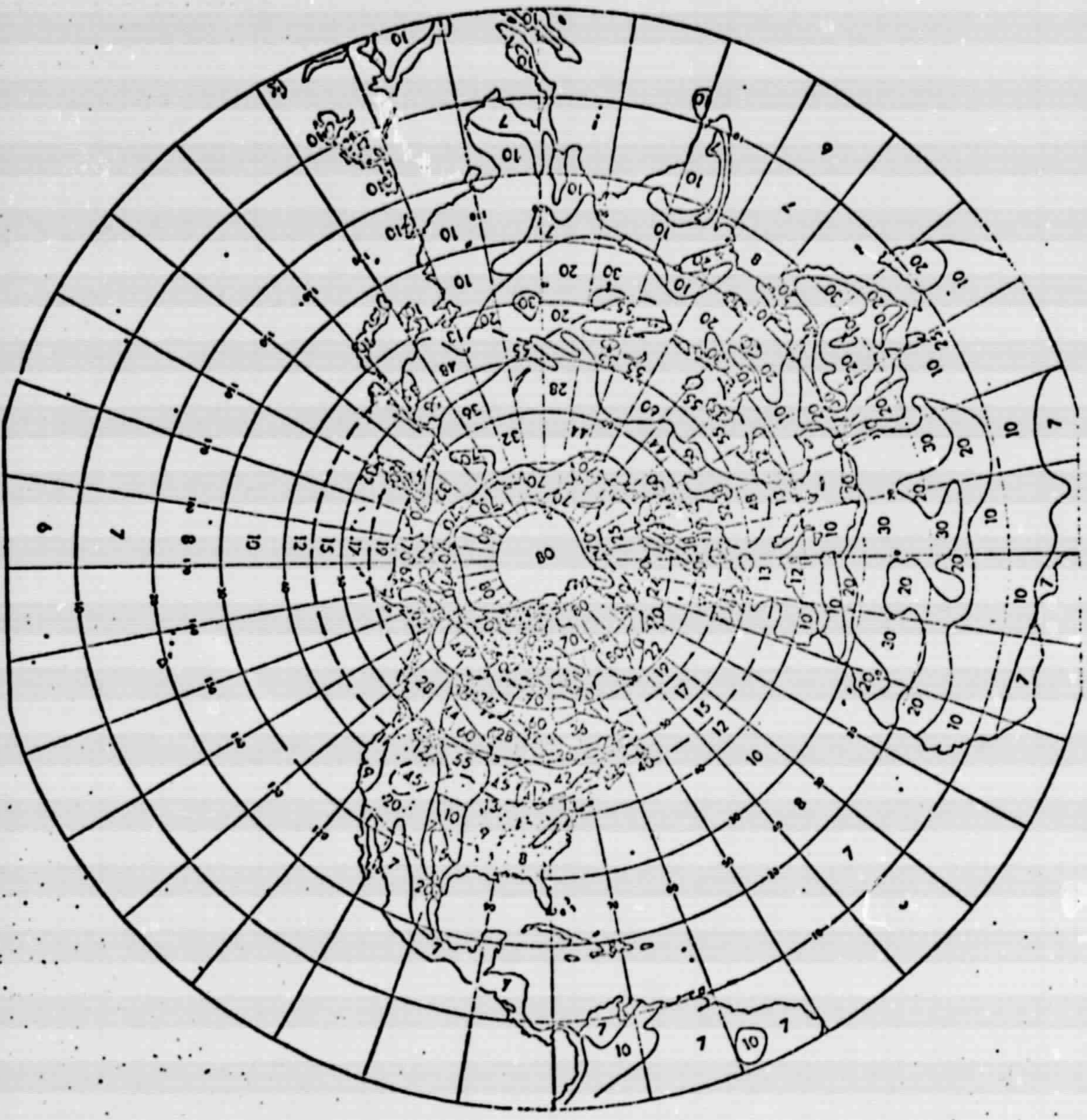

Fig.5. Normal surface albedo, January, Northern Hemisphere. Numbers are albedos in percent. Heavy dashed line over northern oceans is boundary separating ice navigable to ice breakers from that navigable to heavy ships: over land, snow boundary (or line of 50% probability of snow). Light solid line mainly in Artic Ocean, boundary of solid pack ice. Light solid lines over land are discontinuities in albedo, following land-use boundaries. (Taken from Posey and Clapp).

weekly average snow and ice boundary (WASIB) maps for the periods January 26 to February 1, 1976 and February 2 - 8, 1976 are included, figures 6 and 7. These maps are produced by the Satellite Applications Group of NESS (NOAA) using photographs derived from data from NOAA-4 and SMS-1 satellites. Sea ice boundary extents are denoted by circles. The lowest representative surface albedo for the Bering Straits grid box was recorded on January 31, 1976 when sea ice was present. Ice conditions changed the following week according to figure 7. Ice conditions for the other regions remained the same for the two week period.

Four 99 values appear in the Northern Hemisphere. A value of 99 means that no surface representative albedo was recorded for any of the five days. This resulted when an insufficient number of cases comprising the low end peak was present for each of the five days. Mostly cloudy skies over the five days would cause such a condition.

Surface representative albedos for Central America, the northern portions of South America and Africa are in close agreement with those of Posey and Clapp. The higher albedos for the Sahara desert stand out well in both maps, with the satellite derived values slightly higher, 35% as opposed to 30%.

The albedos are also in close agreement in the Arabian Penninsula except for grid points covering both land and

Fig.6. Weekly average snow and ice boundary map for January 26 - February 1, 1976.

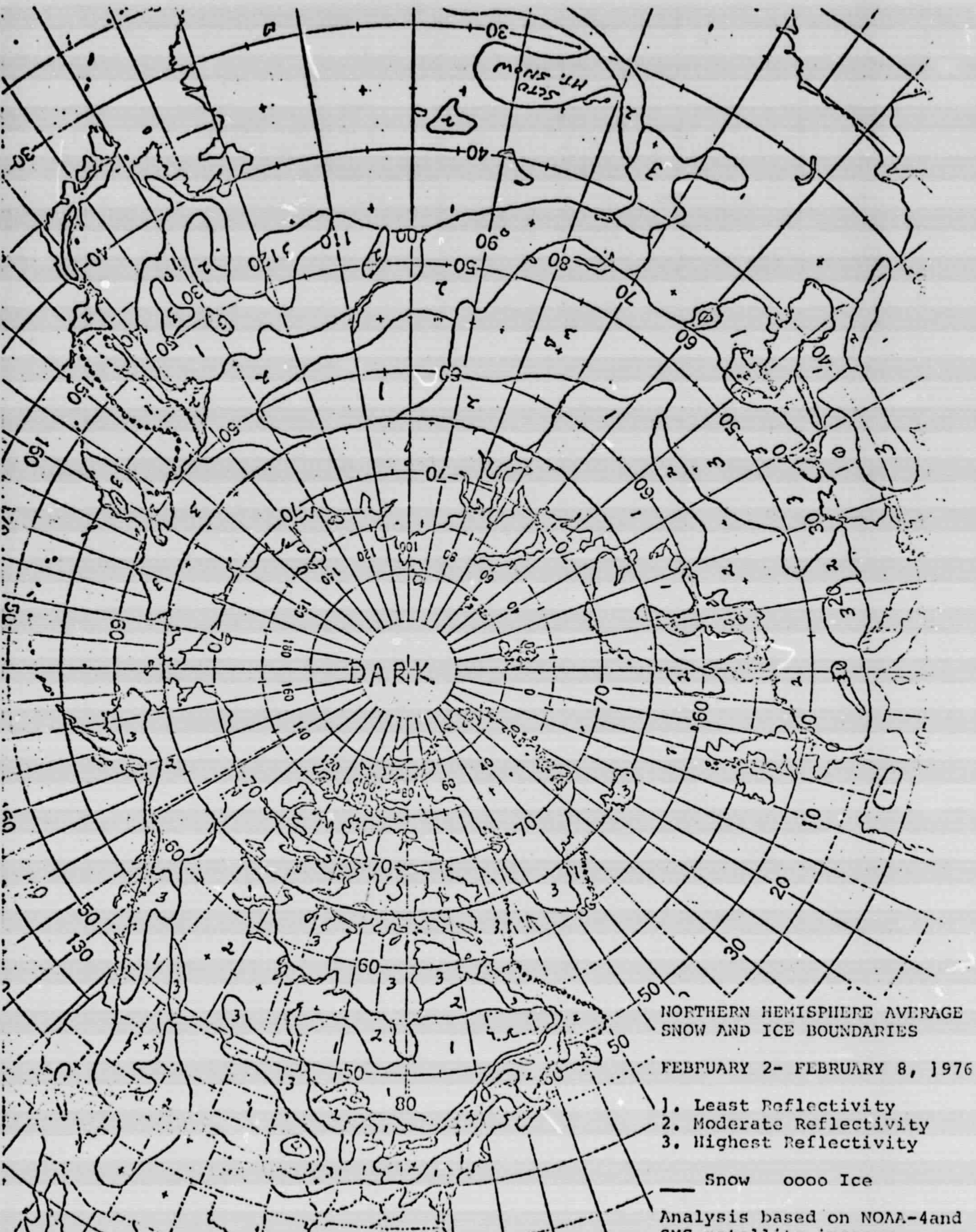

Fig.7. Weekly average snow and ice boundary map for February 2 - 8, 1976.

water. For these the lower albedos for water predominate.

Albedos are somewhat lower in Iran, Afghanistan and Pakistan for the satellite derived maps and slightly higher in India, Southeast Asia and the non desert areas of China. The desert regions of China, exhibit albedos of 20 to 30% in Posey and Clapp whereas they range from 16 to 24% in the satellite derived albedo maps.

The snow boundary extending from the Caspian Sea to the Pacific Ocean on the WASIB maps and on Posey and Clapp, denoted by a dashed line, lie close to each other except the former displays snow cover in the Himalayan Mountains. Albedos to the north of the snow boundary are similar with 40 and 50% albedos near the boundary and decreasing to the upper 20's, 30's and 40% albedos farther to the north on both maps.

In Europe the snow extent on the WASIB maps is more widespread than on the Posey and Clapp map. Higher albedos of 31 to 47% occurred in the non snow covered regions of 13% in Posey and Clapp.

The snow boundary line for North America was fairly close for the Posey and Clapp and the WASIB maps. Judging from the depth of snow on the ground maps, for February 2 and 9, 1976 (figures 8 and 9) extensive melting of snow in the midwest and western plateau regions was indicated for the week preceding February 2, 1976, with widespread snowfall in

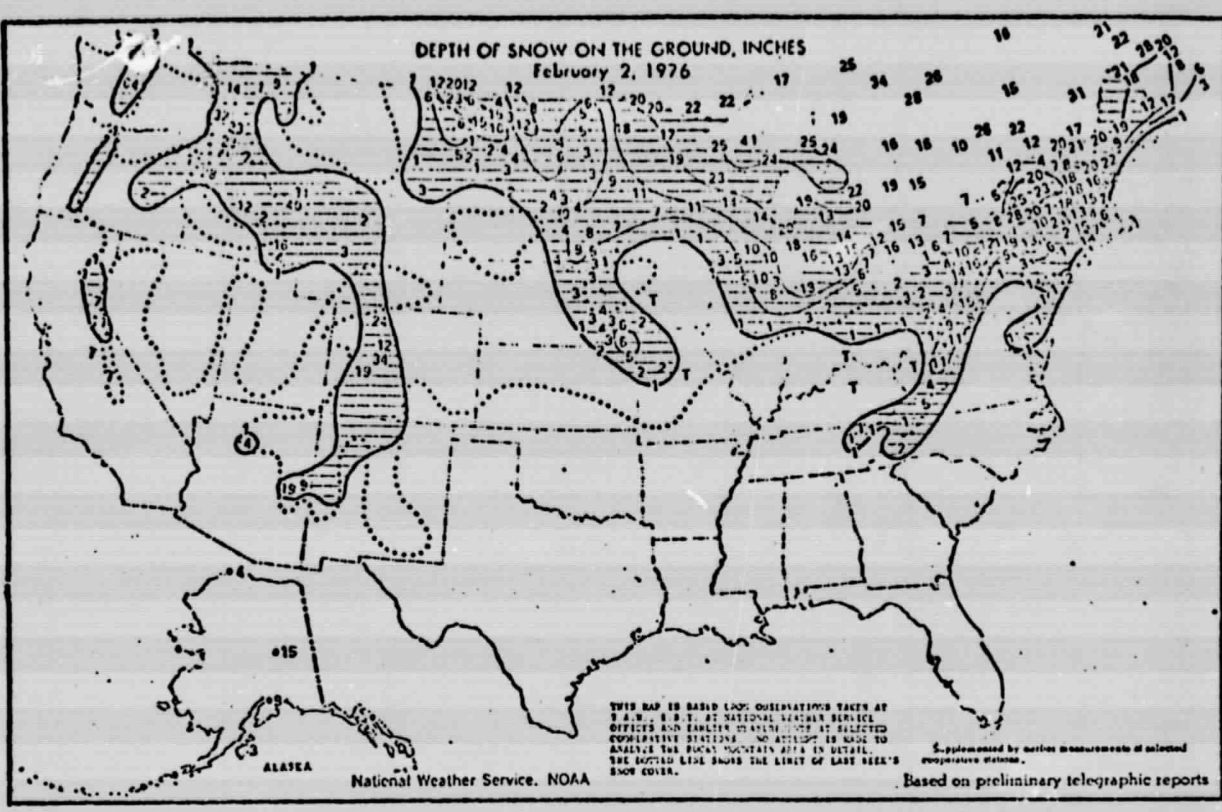

Fig.8. Depth of snow on the ground, February 2, 1976.
(Taken from Weekly Weather and Crop Bulletin, February 3, 1976).

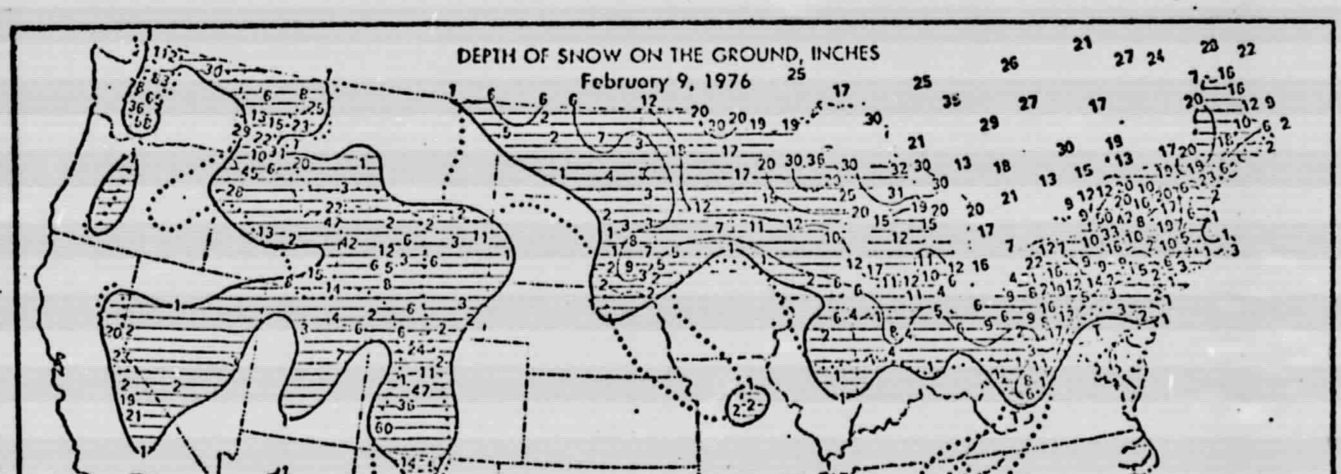

Fig.9. Depth of snow on the ground, February 9, 1976.
(Taken from Weekly Weather and Crop Bulletin, February 10, 1976).

the following week. Melting snow and snow free areas characteristically have lower albedos than the same regions with fresh fallen snow. As expected albedos in the north central U.S. and Rocky Mountain states have lower albedos, 16 and 17%, than 45 and 55% for Posey and Clapp. The non snow covered southern states have identical albedos. The grid boxes in the southwestern states and south into Mexico display differences possibly linked to ground wetness and a mixture of soil types. Except for Hudson Bay, both maps exhibit similar albedos over Canada. Alaska's albedo of 38% is the same for Posey and Clapp except near the southern coast where Posey and Clapp note a 62% albedo region.

Conclusions

The cloud filtering techniques applied to satellite scanning radiometer data in the visible spectrum enabled the production of a global surface albedo map with quite reasonable values. Open water albedos were generally 7 to 11% and increased to 21% in the higher northern latitudes. Three regions with extensive sea ice had albedos of 49 to 59%. Non snow and ice covered land albedos ranged from 7 to 16% with albedos from the mid 20s to 35% for desert regions. Snow covered lands displayed high albedos from the mid 20s to 63%. Albedos for Antarctica were normally high ranging from 80 to the radiometers upper limit of 91%.

Incorrect albedos did, however, still remain in the global albedo map. Disregarding regions of insufficient reflected light due to the tilt of the earth and data retention procedures used on the last pass of the satellite, some unusually high albedos were caused by persistent clouds over the regions for five days, by a combination of clouds and sun glint, and by other not as clearly defined influences. Further study needs to be undertaken using more days for minimum surface albedo retrieval, and a smaller minimum sample size than the 2000 used in this study for a representative surface albedo determination for each grid box.

Nevertheless, a comparison of global albedo maps, one derived from satellite data and the other from surface and aircraft measurements and characteristic albedos for specific land use and land types showed two quite similar maps for all surface conditions.

Acknowledgments

The research reported in this paper was carried out at the Goddard Institute for Space Studies (GISS) under a grant (NGR 33-013-086) from the Goddard Space Flight Center (NASA) to The City College. This work could not have been accomplished without the cooperation and assistance of the staff of GISS, including Robert Jastrow, director, Milton Halem, William Quirk and Roger Van Norton, and also the staff of The National Environmental Satellite Service (NOAA) including Jay Winston, Arnold Gruber and Edward Hoppe. I would like to express my gratitude to my advisor, Jerome Spar for his excellent guidance and encouragement.

References

Budyko, M.I. 1958. Teplovoi balans zemnoi poverkhosti. (The Heat Balance of the Earth's Surface). Gidrometeorologicheskoe izdatel'stvo, Leningrad, 1956 (Translated by Nina A. Stepanova, Office of Climatology, U.S. Weather Bureau, Washington, D.C., 259 pp.).

Chen, T.S. 1975. Monthly minimum and maximum albedos. Unpublished report, 19 pp. National Environmental Satellite Service, NOAA.

Conlan, Edward F. 1973. Operational products from ITOS scanning radiometer data. NOAA Tech. Rept. NESS 52, 57 pp.

Environmental Satellite Imagery, February, 1976. National Oceanographic and Atmospheric Administration. Environmental Data Service, 92 pp.

Flanders, Donald H. and William L. Smith, 1975. Radiation budget data from the meteorological satellites, ITOS 1 and NOAA 1. NOAA Tech. Rept. NESS 72, 21 pp.

Fortuna, Joseph J. and Larry N. Hambrick, 1974. The operation of the NOAA polar satellite system. NOAA Tech. Rept. NESS 60, 1 - 17.

Gruber, Arnold, 1973. Review of satellite measurements of albedo and outgoing long-wave radiation. NOAA Tech. Rept. NESS 48, 13 pp.

Gruber, Arnold, 1974. Calibration of NOAA 2 visible scanning radiometer. Unpublished report, 6 pp., National Environmental Satellite Service, NOAA.

Kung, Ernest C., Reid A. Bryson and Donald H. Lenschow, 1964. Study of a continental surface albedo on the basis of flight measurements and structure of earth's surface cover over North America. Mon. Wea. Rev., 92. 543 - 564.

McClain, E. Paul and Donald F. Baker, 1969. Experimental large-scale snow and ice mapping with composite minimum brightness charts. ESSA Tech. Rept. NESCTM 12, 20 pp.

Posey, Julian W. and Phillip F. Clapp, 1964. Global distribution of normal surface albedo. Geofisica Internacional, 4, 33 - 48.

Quirk, William and Yogish Sud, 1976. Personal Communication.

Raschke, E. and W.R. Bandeen, 1970. The radiation balance of the planet Earth from radiation measurements of the satellite Nimbus II. J. Appl. Meteor., 9, 215 - 238.

Schutz, C. and W.L. Gates, 1972. Supplemental Global Climatic Data: January. The Rand Corp., R-915/1-ARPA, 41 pp.

Schwalb, A., 1972. Modified version of the improved TIROS operational satellite (ITOS D-G). NOAA Tech. Rept. NESS 35, 49 pp.

Sommerville, R.C.J., P.H. Stone, M. Halem, J.E. Hansen, J.S. Hogan, L.M. Druyan, G. Russell, A.A. Lacis, W.J. Quirk and J. Tenenbaum, 1974. The GISS model of the global atmosphere. J. Atmos. Sci., 31, 84 - 117.

Taylor, V. Ray and Jay S. Winston, 1968. Monthly and seasonal mean global charts of brightness from ESSA 3 and ESSA 5 digitized pictures, February, 1967 - February, 1968. ESSA Tech. Rept. NESC 46, 9 pp., and 17 charts.

Vonder Haar, Thomas H. and Verner E. Suomi, 1971. Measurements of the earth's radiation budget from satellites during a five year period. Part 1: Extended time and space means. J. Atmos. Sci., 28, 305 - 314.

Winston, Jay S. and V. Ray Taylor, 1967. Atlas of world maps of long-wave radiation and albedo, for reasons and months based on measurements from TIROS IV and TIROS VII. ESSA Tech. Rept. NESC 43, 32 pp.

Winston, Jay S., 1971. The annual course of zonal mean albedo as derived from ESSA 3 and 5 digitized picture data. Mon. Wea. Rev., 99, 818 - 827.

A P P E N D I X

```
        COMPILER OPTIONS -     NAME=  MAIN,OPT=00,LINECNT=55,SIZE=0400K,
                               SOURCE,EBCDIC,NOLIST,NODECK,LOAD,MAP,NOEDIT,ID,NOXREF
                 C
                 C   TEST 10 HISTOGRAMS ONTO OUTPUT TAPE **FOR MORE THAN ONE INPUT TAPE AT A TIME
                 C
                 C**PROGRAM READS DATA FROM TAPE,PLACES IT INTO HISTOGRAMS OF BRIGHTNESS VALUES
                 C   VS SMOOTHED FREQUENCIES. SEARCHES FOR LOW END FREQUNCY DISTRIBUTION OF 80
                 C   PER CENT TO 35 PER CENT. GIVES MEANS AND 1 STANDARD DEVIATION OF DATA
                 C   FROM B. V. 1 TO IHISE (IHISE CAN POSSIBLY BE 254)
                 C   NBVAL ARRAYS INITIALIZED AS ALL 0 BRIGHTNESS VALUES(DEFAULT)
                 C   CREATES TAPE OF HISTOGRAMS AND LOW END STATISTICS ON A 25 X 25 GRID
                 C   FOR 5 DAYS, NORTHERN OR SOUTHERN HEMISPHERE.
                 C
   ISN 0002            DIMENSION IAFREQ(256,25),ISFREQ(256,25),LENDSF(256),IFFREQ(256)
   ISN 0003            LOGICAL*1 NBVAL(6400,25),NT(8192)
   ISN 0004            DATA NUMREC,N,IFSTDA,FMEAN,FSDEV,NUMF,IFHISB,IFHISE,MODEF,
                     1 FPCENT/0,25,1190,99.,0.,0.,0,0,0,0./
                 C
                 C POSITION OUTPUT TAPE
   ISN 0005          4 DO 5 LK=1,700
   ISN 0006          5 READ(9,END=6)IDAY
                 C
                 C   READS PASSED UNWANTED INPUT DATA
   ISN 0007          6 NUMREC=0
   ISN 0008            DO 35 K=1,12
   ISN 0009            NUMREC=NUMREC+1
   ISN 0010            CALL VREDE(-8,NT,NBYTES,IOK)
   ISN 0011         35 IF(IOK.NE.1) WRITE(6,40)NUMREC,NBYTES,IOK
   ISN 0013         40 FORMAT(/,/,/,' ****VREDE ERROR ON RECORD NO.',I3,3X,'BYTES READ=',
                      1 I5,3X,'IOK=',I2)
                 C
   ISN 0014            DO 25 J25=1,25
                 C
                 C   READ DATA INTO 25 NBVAL ARRAYS
   ISN 0015            I6400=-160
   ISN 0016            DO 55 KJ=1,40
   ISN 0017            I6400=I6400+160
   ISN 0018            IVALB=-110
   ISN 0019            IIVALB=3586
   ISN 0020            NUMREC=NUMREC+1
   ISN 0021            CALL VREDE(-8,NT,NBYTES,IOK)
   ISN 0022            IF(IOK.NE.1) WRITE(6,40)NUMREC,NBYTES,IOK
   ISN 0024            DO 65 I25=1,25
   ISN 0025            IVALB=IVALB+160
   ISN 0026            IVALE=IVALB+158
   ISN 0027            NA=0
   ISN 0028            DO 75 KC=IVALB,IVALE,2
   ISN 0029            NA=NA+1
   ISN 0030         75 NBVAL(I6400+NA,I25)=NT(KC)
   ISN 0031            IIVALB=IIVALB+160
   ISN 0032            IIVALE=IIVALB+158
   ISN 0033            DO 85 KD=IIVALB,IIVALE,2
   ISN 0034            NA=NA+1
   ISN 0035         85 NBVAL(I6400+NA,I25)=NT(KD)
   ISN 0036         65 CONTINUE
```

```
          C
          C  SORT B.V. IN ARRAYS INTO ACTUAL FREQUENCY DISTRIBUTION ARRAY IAFREQ
ISN 0038        DO 175 LD=1,N
ISN 0039        DO 115 LE=1,256
ISN 0040    115 IAFREQ(LE,LD)=0
ISN 0041    175 CONTINUE
ISN 0042        DO185 LA=1,N
ISN 0043        DO145 LC=1,6400
ISN 0044        DO155 KFREQ=1,256
ISN 0045        KBV=KFREQ-1
ISN 0046        IF(KBV.NE.NBVAL(LC,LA)) GO TO 155
ISN 0048        IAFREQ(KFREQ,LA)=IAFREQ(KFREQ,LA)+1
ISN 0049        GO TO 145
ISN 0050    155 CONTINUE
ISN 0051    145 CONTINUE
ISN 0052    185 CONTINUE
          C
          C  APPLY HEAVY SMOOTHER ON ACTUAL FREQUENCIES
ISN 0053        DO 43 NG=1,N
ISN 0054        IF(IAFREQ(256,NG).GT.6200) GO TO 43
ISN 0056        DO 47 NH=1,256
ISN 0057        ISFREQ(NH,NG)=IAFREQ(NH,NG)
ISN 0058        IF(NH.EQ.2)ISFREQ(NH,NG)=(IAFREQ(NH,NG)+IAFREQ(NH+1,NG))/2
ISN 0060        IF(NH.EQ.254)ISFREQ(NH,NG)=(IAFREQ(NH,NG)+IAFREQ(NH-1,NG))/2
ISN 0062        IF(NH.GT.2.AND.NH.LT.254)
               1  ISFREQ(NH,NG)=(IAFREQ(NH-1,NG)+IAFREQ(NH,NG)+IAFREQ(NH+1,NG))/3
ISN 0064     47 CONTINUE
ISN 0065     43 CONTINUE
          C
          C  WRITE OUT HISTOGRAMS
ISN 0066        DO 53 NI=1,N
ISN 0067        WRITE(6,50) J25,NI,IFSTDA
ISN 0068     50 FORMAT(/,/,/,' ***HISTOGRAM    J ROW=',I3,4X,'I COLUMN=',I3,4X,
               1 'DAY=',I5)
ISN 0069        IF(IAFREQ(256,NI).LE.6200) GO TO 141
ISN 0071        WRITE(6,58)(IAFREQ(256,NI))
ISN 0072     58  FORMAT(/,4X,'IAFREQ(256,I COLUMN)=',I5)
ISN 0073        WRITE(9)IFSTDA,FMEAN,(IAFREQ(LH,NI),LH=1,256),IFFREQ,FSDEV,FSDEV,
               1 NUMF,IFHISB,IFHISE,MODEF,MODEF,FPCENT
ISN 0074        GO TO 53
          C
          C  PLACE 1ST 80,70,60,50,45,40,35 PER CENT OF DATA INTO ARRAY LENDSF
          C  ARRAY LENDSF EXTENDS FROM B.V. 1 UP TO A POSSIBLE B.V. OF 254
ISN 0075    141 PCENT=.80
ISN 0076    142 IPCENT=PCENT*6400
ISN 0077        ISUM=0
ISN 0078        IHISE=0
ISN 0079        DO 103 KM=2,255
ISN 0080        KBV=KM-1
ISN 0081        LENDSF(KM)=ISFREQ(KM,NI)
ISN 0082        ISUM=ISUM+LENDSF(KM)
          C
          C  SEARCH LENDSF ARRAY (LOW B.V. TO HIGH) FOR FIRST B.V. WITH FREQ.GE.4
ISN 0083        IF(IHISB.EQ.0.AND.LENDSF(KM).GE.4) IHISB=KBV
ISN 0085        IF(ISUM.GE.IPCENT) GO TO 105
ISN 0087    103 CONTINUE
```

```
                   C
                   C  SEARCH AND PLACE HIGHEST FREQUENCIES OF LENDSF ARRAY INTO
                   C  MODESF. LOWEST BRIGHTNESS VALUE SELECTED FIRST FOR EQUIVALENT FREQUENCIES.
                   C  MODEBV CORRESPONDS TO A MODAL BRIGHTNESS VALUE
ISN 0088             105 MODESF=LENDSF(2)
ISN 0089                 MODEBV=1
ISN 0090                 KN=KBV+1
ISN 0091                 DO 113 KP=2,KN
ISN 0092                 IF(MODESF     .GE.LENDSF(KP)) GO TO 113
ISN 0094                 MODESF     =LENDSF(KP)
ISN 0095                 MODEBV     =KP-1
ISN 0096             113 CONTINUE
                   C
                   C  ZERO MODAL FREQUENCY CHECK      (ALL B.V.=0 FOR ENTIRE ARRAY)
ISN 0097                 IF(MODESF     .NE.0) GO TO 126
ISN 0099                 WRITE(6,125)
ISN 0100             125 FORMAT(/, 4X,'MODAL FRECUENCY ECUALS 0  ALL B.V. FOR GRID BOX=0')
ISN 0101                 WRITE(9)IFSTDA,FMEAN,(IAFREQ(LH,NI),LH=1,256),IFFREQ,FSDEV,FSDEV,
                       1 NUMF,IFHISB,IFHISE,MODEF,MODEF,FPCENT
ISN 0102                 GO TO 52
                   C
                   C  TO CORRECT IHISB IF FIND 2 ADJACENT SMOOTHED FREQUENCIES OF 0 BETWEEN IHISB
                   C  AND MODAL B.V.
ISN 0103             126 IF(MODEBV.EQ.1) GO TO 124
ISN 0105                 IDIFF=MODEBV-IHISB-2
ISN 0106                 IHISCK=MODEBV+1
ISN 0107                 DO 195 LF=1,IDIFF
ISN 0108                 IHISCK=IHISCK-1
ISN 0109                 IF(ISFREQ(IHISCK,NI).EQ.0.AND.ISFREQ(IHISCK-1,NI).EQ.0) GO TO 200
ISN 0111             195 CONTINUE
ISN 0112                 GO TO 124
ISN 0113             200 DO 205 LG=IHISCK,MODEBV
ISN 0114             205 IF(ISFREQ(LG,NI).GE.4) GO TO 210
ISN 0116             210 IHISB=LG-1
                   C
                   C  EXTENT OF LOW END HISTOGRAM
ISN 0117             124 IHISE=2*MODEBV    -IHISB
ISN 0118                 IF(PCENT.LT..37) GO TO 148
                   C
                   C  CHECK FOR CLEAR SKIES HISTOGRAMS(HIGH FREQ OVER SMALL RANGE).LE.52))
ISN 0120                 IF((IHISE-IHISB).LE.52) GO TO 148
ISN 0122                 IF(PCENT.GT..52)PCENT=PCENT-0.05
ISN 0124                 PCENT=PCENT-0.05
ISN 0125                 GO TO 142
                   C  IHISE CAN BE B.V. 254
ISN 0126             148 IF(IHISE.GT.254) IHISE=254
                   C
                   C  COMPUTE MEAN AND STANDARD DEVIATION OF LOW END (LOW BRIGHTNESS
                   C  VALUES) HISTOGRAM
ISN 0128                 SUM=0.
ISN 0129                 DEV=0.
ISN 0130                 NUM=0
                   C
                   C  MEANS AND S.D. FROM FREQUENCIES OF B.V. 1 TO IHISE (IHISE CAN BE 254)
ISN 0131                 DO 127 KS=1,IHISE
ISN 0132                 KU=KS+1
ISN 0133                 SUM=SUM+KS*ISFREQ(KU,NI)
ISN 0134                 NUM=NUM+ISFREQ(KU,NI)
ISN 0135             127 DEV=DEV+KS**2*ISFREQ(KU,NI)
```

```
                C
                C   NO STATISTICS FCR HISTOGRAMS WITH A SUM OF FREQUENCIES .LT. 30C
ISN C136              IF(NUM.GE. 300) GO TC 165
ISN 0138              WRITE(6,16C)     IHISB,IHISE,NUM
ISN 0139          160 FCRMAT(/,4X,'SUM OF FREQUENCIES.LT.300',/,4X,  'IHISB=',I4,
                    1 '    IHISE=',I4,'    SUM CF FREQ IN LCW END STATS PORTION=',I4)
ISN C140              WRITE(9)IFSTDA,FMEAN,(IAFREQ(LH,NI),LH=1,256),IFFREQ,FSDEV,FSDEV,
                    1 NUM,IHISB,IHISE,MODEBV,MCDESF,PCENT
ISN C141              GO TC 53
ISN 0142          165 XMEAN=SUM/NUM
ISN 0143              AMEAN=(XMEAN*0.3601)
ISN C144              DIFF=NUM*DEV-SUM**2
ISN 0145              DIV=DIFF/(NUM*(NUM-1))
ISN C146              SDEV=SQRT(DIV)
ISN C147              ASDEV1=(XMEAN-SDEV)*0.36C1
ISN C148              ASDEV2=(XMEAN+SDEV)*C.36C1
ISN 0149              WRITE(6,170)AMEAN,ASDEV1,ASDEV2,IHISB,MODEBV,IHISE,MCDESF,NUM,
                    1 PCENT
ISN 0150          170 FORMAT(/,  4X,'MEAN ALBEDO(=',F6.2,4X,'ALBEDO RANGE(1 STAN.DEV)=',
                    1 F6.2,' TO',F7.2/,4X,'IHISB=',I4,'    MODEBV=',I4,'    IHISE=',I4,
                    2 '    MODESF=',I5,'    NUM=',I5,'    P CENT OF DATA SEARCHED=',F4.2/)
ISN 0151              WRITE(9)IFSTDA,AMEAN,(IAFREQ(LH,NI),LH=1,256),
                    1(ISFREQ(LI,NI),LI=1,256),ASDEV1,ASDEV2,
                    2 NUM,IHISB,IHISE,MCDEBV,MCDESF,PCENT
ISN 0152           53 CONTINUE
ISN 0153              WRITE(6,80)NUMREC,I640C,NA,IVALB,IVALE,IIVALB,IIVALE
ISN 0154           80 FCRMAT(/,/,' LAST RECCRD READ=',I5,3X,'I6400=',I5,3X,'NA=',I4,/,
                    1 ' IVALB=',I5,3X,'IVALE=',I5,3X,'IIVALB=',I5,3X,'IIVALE=',I5,/,
                    2 ' *************************************************************')
ISN C155           25 CONTINUE
ISN C156              ENDFILE 9
ISN C157              PAUSE ' MCUNT NEXT TAPE(FF) CN LOG 8'
ISN C158              IFSTDA=IFSTDA+1
ISN C159              IF(IFSTDA.LE.1193) GO TC 6
ISN C161              STOP
ISN C162              END
```